GSA Data Repository 2015288

Are the large filamentous microfossils preserved in Messinian gypsum colorless sulfide-oxidizing bacteria?

Francesco Dela Pierre, Marcello Natalicchio, Simona Ferrando, Roberto Giustetto, Daniel Birgel, Giorgio Carnevale, Susanne Gier, Francesca Lozar, Domenica Marabello, and Jörn Peckmann

This document describes the methods, shows tabulated data on the composition of the studied filaments and of detrital mineral grains, scanning electron microscope (SEM) images and energy-dispersive X-ray spectrometer (EDS) spectra of the analyzed material, X-ray diffraction (XRD) patterns and the interpretation of the micro-Raman spectra obtained from isolated filaments (Fig. 3).

Sampling and methodology

Messinian gypsum crystals were sampled from unweathered outcrop faces from three sections: Narzole (44.58829° N, 7.867800° E), Monucco (45.060079° N, 7.939612° E) and Banengo (45.072350° N, 8056464° E). A total of 20 petrographic sections, about 1 mm thick, were obtained and studied under an optical microscope. Fluorescence intensity was evaluated using a Nikon microscope equipped with a B2-a filter block (illumination source with an excitation wavelength of 450-490 nm). Filaments were isolated by dissolving cm-sized gypsum fragments from three samples, obtained by cleaving the crystals along the {010} face with a razor blade. The fragments were left for 72 h in ultrapure water heated to 40°C. SEM/EDS semiquantitative elemental analyses were performed on five carbon-coated representative sections and on isolated filaments, using a SEM Cambridge Instruments Stereoscan 360 equipped with an Oxford Instruments Link System microprobe (Table DR1). The Mg, Al, Si, K and Fe contents (atomic %)

of the honey-comb structure of the filament walls and the detrital micas (Figs. DR1, DR2, DR3) were measured. Micro-Raman spectra were acquired from the minerals composing the filaments with an integrated micro/macro-Raman LABRAM HRVIS (Horiba Jobin Yvon Instruments) provided by the Interdepartmental Center "G. Scansetti" and by the Compagnia di San Paolo, Torino, Italy; in particular, 35 spectra were collected from the tiny iron sulfide grains observed within them. Excitation lines at 532 nm (solid-state Nd laser and 80 mW of emission power) and 633 nm (HeNe laser and 20 mW of emission power) were used with Edge filters and a grating of 600 grooves/mm. The laser spot size ranged from 2 to 8 μm. One to six accumulations in the time span of 20–60 s were collected for each spectrum and D1, D2 or D3 filters have been alternatively inserted. Calibration was performed using the 520.6 cm^{-1} Si band. The Raman spectrum from the gypsum hosting the filaments shows the typical strong peaks of the (SO_4^{2-}) vibrations at 1008, 494 and 414 cm^{-1} (Frezzotti et al., 2011) (Fig. 3). Spectra obtained from the filaments are overlain by sulfate ions peaks. A spectrum obtained for an opaque crystal enclosed in a filament is representative of pyrite (Fig. 3). The strong peak at 340 cm^{-1} is due to S displacement perpendicular to the (S_2^{2-}) dimer axis (E_g); the peak at 376 cm^{-1} is due to stretching vibration of the (S_2^{2-}) dimer in phase throughout the crystal (A_g), whereas the weaker band at 426 cm^{-1}, only locally observed, is due to various vibrational and stretching vibrations or to their combinations (T_g) (Blanchard et al., 2005; Toniazzo et al., 1999). The Raman shift of these bands increases consistently with increasing pressure (Mori and Takahashi, 1987; Blanchard et al., 2005). The habit of pyrite crystals and the low values of the corresponding Raman shift indicate their diagenetic rather than detrital source. Another spectrum obtained from an opaque crystal enclosed in a filament is typified by a broad band at 470 cm^{-1} (Fig. 3). The low Raman shift and the absence of other peaks exclude the presence of elemental sulfur (S_8: Pasteris et al., 2001). Similar bands in the 440 and 480 cm^{-1} wavelength region (main at 470 cm^{-1}) have been attributed to polysulfide (S_n^{2-}; e.g., Khan et al., 2011). In particular, a vibration frequency near 465 cm^{-1} has been attributed to polysulfide, possibly S_3^{2-} (Toniazzo et al., 1999; Berg et al., 2014). Other spectra obtained from the filaments are

representative of poorly organized (i.e., amorphous) carbonaceous material. These spectra show two strong broad bands centered at about 1365 and 1600 cm^{-1}, which represent the disordered band (D-band; excitation light source at 532 nm) and the sp2 bonds (i.e., the ordered band, also called G-band) of disordered carbon (Frezzotti et al., 2011), respectively.

X-ray diffraction (XRD) analyses were performed separately on the isolated filaments by mixing uncrushed specimens with small drops (about 0.5 mm) of a non-drying immersion hydrocarbon based oil for microscopy (type B, code 1248, Cargille Laboratories) and mounting them on a glass capillary. XRD patterns (Fig. DR 4) were collected using an Oxford Diffraction Gemini R Ultra diffractometer with mirror monochromatized Cu-Kα radiation (Enhanced Ultra technology; λ=1.5418 Å) in the 2.8 to 70° 2θ range by rotating the samples of 60° during collection with an exposure time of 60 s. The CrysAlisPro package (CrysAlisPro, Agilent Technologies, Version 1.171.36.28) was used for data integration. The Diffrac Plus (2005) software (EVA 11, 0 0, 3) was used for identification of mineral phases.

MATERIAL	SAMPLE	Type of sample	Locality	Mg atomic %	Al atomic%	Si atomic %	K atomic%	Fe atomic%	Total
Filament	BG1	P.S.	Banengo	1.3	9.9	20.2	2.8	1.6	70.2
	BG1	P.S.	Banengo	1.3	4.5	10.2	1.6	1.1	48.4
	BG1	P.S.	Banengo	0.9	7.0	24.0	3.2	1.0	69.0
	BG1	P.S	Banengo	1.0	3.8	9.0	0.7	1.6	64.5
	BG1	P.S.	Banengo	2. 7	5.6	10.5	0.5	16.2	58.3
	BG1	P.S.	Banengo	2.2	9.1	19.8	4.4	1.7	68.1
	BG1	P.S.	Banengo	0.6	2.0	5.0	1.0	1.7	28.8
	BG1	P.S.	Banengo	0.3	1.7	4.4	0.8	0.7	48.4
	BG1	P.S.	Banengo	0.6	4.5	9.0	1.6	0.4	38.2
	BG1	P.S.	Banengo	0.6	3.7	9.6	0.8	0.4	32.7
	BG1	P.S.	Banengo	1.9	3.8	7.6	1.3	2.1	34.8
	BG1	P.S.	Banengo	1.2	2.8	13.6	1.1	0.7	30.5
	BG1	P.S.	Banengo	1.3	3.7	9.2	0.4	0.2	29.3
	BG1	P.S.	Banengo	0.2	0.7	2.4	0.0	0.1	37.8
	BG4	P.S.	Banengo	0.3	1.6	3.8	0.7	0.8	23.5
	BG4	P.S.	Banengo	0.1	0.6	1.3	0.2	0.1	58.1
	BG4	P.S.	Banengo	0.4	2.2	4.9	0.6	0.8	31.0
	BG4	P.S.	Banengo	0.2	0.8	1.5	0.1	0.2	27.9
	BG4	P.S.	Banengo	0.1	2.1	6.5	1.6	0.3	42.5
	BG4	P.S.	Banengo	0.6	2.0	10.1	0.3	0.3	93.0
	BG4	P.S.	Banengo	0.3	0.5	1.2	0.1	0.2	80.1
	BG4	P.S.	Banengo	2.0	4.3	14.0	0.6	1.7	81.5
	BG4	P.S.	Banengo	0.3	1.4	3.1	0.5	0.7	26.7
	BG4	P.S.	Banengo	1.8	7.5	12.6	1.5	1.1	76.3

	BG4	P.S.	Banengo	0.1	0.5	1.2	0.1	0.0	71.7
	BG4	P.S.	Banengo	0.5	2.5	6.4	0.5	0.3	86.5
	BG4	P.S.	Banengo	0.9	2.1	3.6	0.2	3.0	83.3
	BG4	P.S.	Banengo	1.7	6.0	12.9	1.2	1.1	73.0
	BG4	P.S.	Banengo	1.1	4.8	15.9	1.1	0.7	63.0
	BG4	P.S.	Banengo	3.0	6.2	12.2	1.4	3.4	63.2
	BG4	P.S.	Banengo	1.2	6.0	11.9	1.6	1.1	84.3
	BG4	P.S.	Banengo	4.4	5.6	9.4	1.8	3.9	79.0
	BG4	P.S.	Banengo	1.7	3.3	6.3	0.7	0.9	86.6
	BG4	P.S.	Banengo	0.6	6.4	16.9	4.6	0.7	59.7
	BG4	P.S.	Banengo	1.4	8.8	29.6	4.4	7.9	19.7
	BG4	I.F.	Banengo	2.4	5.2	9.2	0.7	2.4	102.6
	BG4	I.F.	Banengo	0.5	2.2	5.3	1.1	1.8	54.1
	Gcuc1	P.S	Moncucco	1.0	1.6	3.5	0.5	0.6	36.9
	Gcuc1	P.S	Moncucco	0.2	0.6	1.7	0.0	0.4	15.9
	Gcuc1	P.S	Moncucco	2.3	7.1	19.2	2.3	2.9	31.2
	Gcuc1	P.S	Moncucco	0.3	1.1	2.9	0.4	0.7	27.1
	Gcuc1	P.S	Moncucco	0.5	1.7	4.5	0.5	0.8	54.4
	Gcuc1	P.S	Moncucco	1.9	7.7	20.3	2.6	3.1	47.9
	Gcuc1	P.S	Moncucco	1.3	4.7	11.6	1.3	1.6	61.5
	Gcuc1	P.S	Moncucco	1.4	5.8	18.8	4.2	6.7	36.6
	Gcuc1	P.S	Moncucco	2.0	8.4	20.6	2.3	3.1	56.6
	Gcuc1	P.S	Moncucco	1.2	5.3	13.6	1.6	2.3	57.9
	Gcuc1	P.S	Moncucco	0.9	4.7	13.5	2.2	4.7	35.1
	Gcuc1	P.S	Moncucco	1.4	6.6	13.9	2.4	1.6	83.1
	Gcuc1	P.S	Moncucco	0.2	0.9	2.3	0.9	0.9	27.8
	Gcuc1	P.S	Moncucco	1.7	6.1	24.1	2.0	2.0	69.2
	Gcuc1	P.S	Moncucco	1.9	6.4	23.6	2.0	1.7	79.3
	Gcuc1	P.S	Moncucco	1.9	11.5	19.0	4.7	1.0	75.6
	Gcuc1	P.S	Moncucco	3.4	9.8	18.0	3.4	1.5	70.5
	Gcuc2	I.F.	Moncucco	5.0	4.9	8.5	0.4	3.5	118.4
	Gcuc2	I.F.	Moncucco	7.4	7.4	8.6	0.2	8.7	75.5
	Gcuc2	I.F.	Moncucco	3.2	7.3	10.9	0.6	5.4	96.1
	NZ3	P.S	Narzole	3.9	9.4	14.8	5.3	1.3	11.6
	NZ3	P.S	Narzole	3.0	8.7	19.5	2.9	3.2	11.2
	NZ3	P.S	Narzole	2.4	10.6	18.2	4.8	2.5	12.0
	NZ3	P.S	Narzole	2.6	6.3	13.9	3.5	4.6	11.0
	NZ3	P.S	Narzole	1.7	10.8	19.1	3.6	1.7	7.0
	NZ3	P.S	Narzole	0.9	3.7	10.0	2.8	0.8	13.0
	NZ3	I.F.	Narzole	1.1	9.6	15.8	4.0	1.7	88.1
	NZ3	I.F.	Narzole	1.6	7.3	14.8	1.9	1.0	97.9
	NZ3	I.F.	Narzole	1.1	7.2	15.3	1.6	0.7	99.7
	NZ3	I.F.	Narzole	1.1	10.1	15.8	4.2	1.7	88.3
	NZ3	I.F.	Narzole	1.3	4.7	15.9	1.5	1.7	54.1
	NZ3	I.F.	Narzole	0.9	2.9	7.9	0.4	1.1	186.0
Detrital mica	BG4	P.S	Banengo	1.4	2.5	4.8	1.4	2.7	55.3
	BG4	P.S	Banengo	5.6	5.0	7.0	0.0	3.7	73.2
	BG4	P.S	Banengo	0.7	9.9	12.6	3.2	0.2	75.5
	BG4	P.S	Banengo	3.1	4.4	7.7	1.5	5.3	44.0
	BG4	P.S	Banengo	1.1	1.9	1.8	0.1	2.3	67.9
	BG4	P.S	Banengo	3.1	4.5	8.3	1.5	5.1	58.6
	BG4	P.S	Banengo	1.0	7.8	11.4	3.1	0.5	71.7
	BG4	P.S	Banengo	0.1	1.2	1.4	0.3	0.1	72.2
	BG4	P.S	Banengo	0.3	6.8	7.0	1.6	0.2	75.3
	BG4	P.S	Banengo	0.1	8.3	8.6	1.7	0.1	83.6
	BG4	P.S	Banengo	7.1	3.5	4.3	0.0	1.3	63.0
	BG4	P.S	Banengo	5.3	2.9	3.2	0.0	0.8	73.4
	BG4	P.S	Banengo	1.1	10.2	13.8	3.3	0.5	73.1

BG4	P.S	Banengo	0.2	7.6	7.8	1.8	0.2	60.7
Gcuc1	P.S	Moncucco	2.1	11.7	17.4	6.0	2.1	62.4
Gcuc2	P.S	Moncucco	1.5	11.7	17.9	7.8	1.1	69.1
Gcuc2	P.S	Moncucco	1.8	10.9	16.6	5.3	1.3	65.4
Gcuc2	P.S	Moncucco	1.5	12.1	17.7	7.3	1.3	68.7

Table DR1: Mg, Al, Si, K and Fe content of the honey-comb structure composing the filament wall and of detrital mica grains. P.S: petrographic section; I.F.: isolated filament

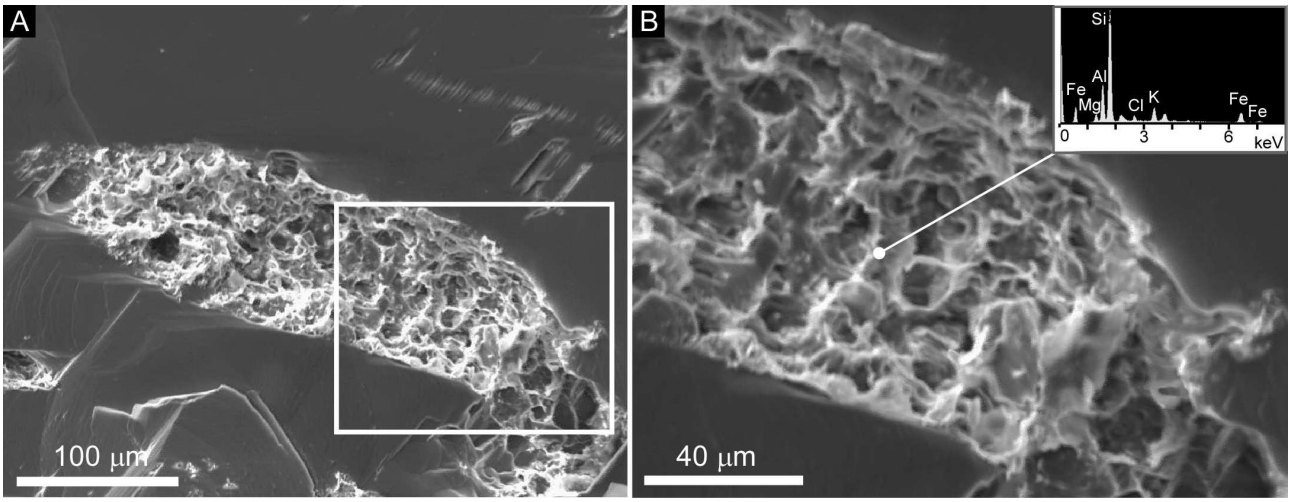

Fig. DR1: A) SEM image of a petrographic section showing a filament enclosed in gypsum (Sample GCuc 1) and (B) detail of the honey-comb structure of its wall; an EDS spectrum is shown in the right box.

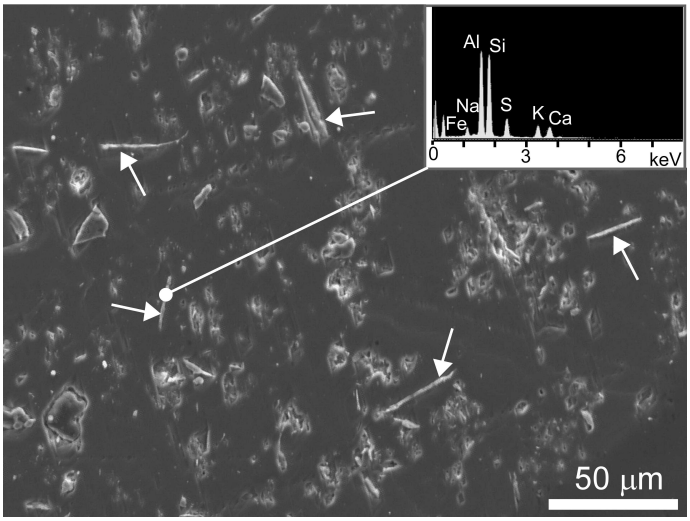

Fig. DR2: SEM image of some detrital mica grains (white arrows) enclosed in gypsum (petrographic section) and EDS spectrum of one spot analysis (sample BG4).

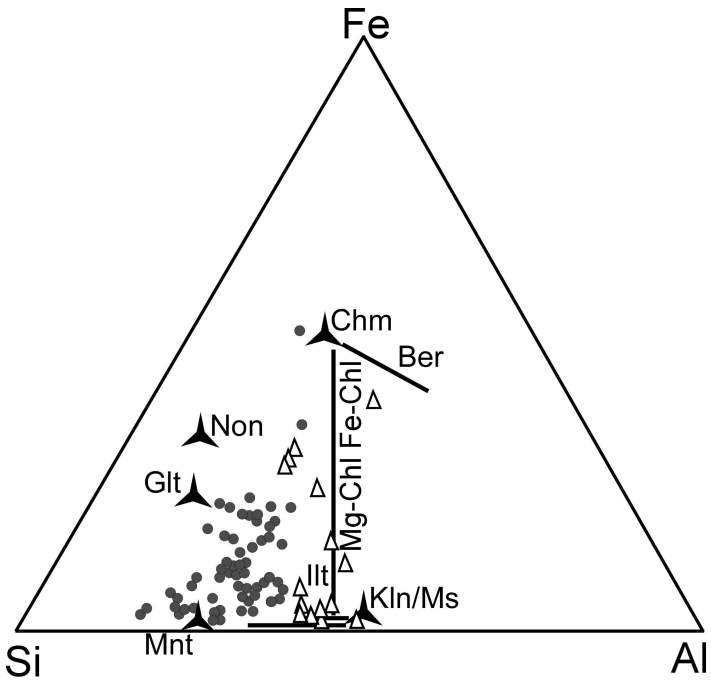

Fig. DR3: Ternary Si-Fe-Al diagram (atomic%) reporting the composition of the filament clay (gray dots) and of detrital micas (triangles). Several ideal phyllosilicates, including illite (Ilt), chamosite (Chm), berthierine (Ber), glauconite (Glt), nontronite (Non), montmorillonite (Mnt), kaolinite (Kln), muscovite (Ms), Mg chlorite (Mg-Chl), and Fe-chlorite (Fe-Chl) are shown.

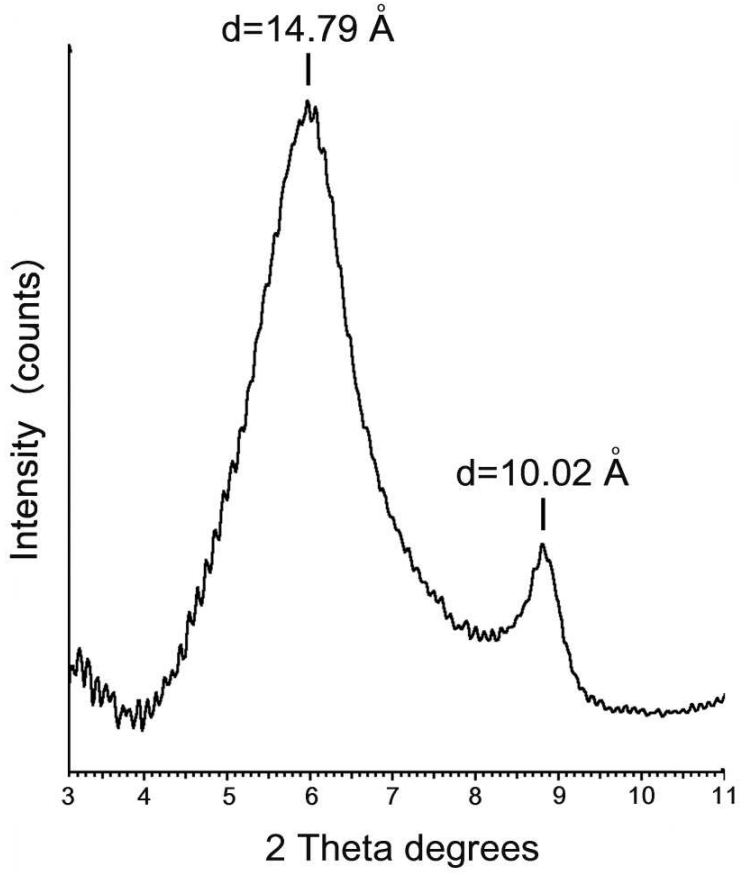

Fig. DR4: XRD pattern of isolated filaments from Narzole. Presence of smectites is evidenced by the broad band at d = 14.79 Å. The weaker reflection at d = 10.02 Å corresponds to illite.

REFERENCES CITED

Berg, J.S., Schwedt, A., Kreutzmann, A.C., Kuypers, M.M.M., and Milucka, J., 2014, Polysulfides as intermediates in the oxidation of sulfide to sulfate by *Beggiatoa* spp: Applied and Environmental Microbiology, v. 80, p. 629–636, doi:10.1128/AEM.02852-13.

Blanchard, M., Alfredsson, M., Brodholt, J., Price, G.D., Wright, K., and Catlow, C.R.A., 2005, Electronic structure study of the high-pressure vibrational spectrum of FeS_2 pyrite: The Journal of Physical Chemistry B, v. 109, p. 22067–22073, doi: 10.1021/jp053540.

Diffrac Plus Evaluation Package, 2005. Copyright © SOCABIM 1996-2005.

Frezzotti, M.L., Tecce, F., and Casagli, A., 2011, Raman spectroscopy for fluid inclusion analysis: Journal of Geochemical Exploration, v. 112, p. 1–20, doi: 10.1016/j.gexplo.2011.09.009.

Khan, S.A., Hughes, R.W., and Reynolds, P.A., 2011, Raman spectroscopic determination of oxoanions in aqueous polysulfide electrolyte solutions: Vibrational Spectroscopy, v. 56, p. 241–244, doi:10.1016/j.vibspec.2011.03.001.

Mori, N., and Takahashi, H., 1987, Raman and reflection spectra of pyrite system under high pressure, *in,* Manghnani, M.H., and. Syono, Y, eds, High-pressure research in mineral physics: Washington, D.C., American Geophysical Union, p. 341–345.

Pasteris, J.D., Freeman, J.J., Goffredi, S.K., and Buck, K.R., 2001, Raman spectroscopic and laser scanning confocal microscopic analysis of sulfur in living sulfur-precipitating marine bacteria: Chemical Geology, v. 180, p. 3–18, doi:10.1016/S0009-2541(01)00302-3.

Toniazzo, V., Mustin, C., Portal, J.M., Humbert, B., Benoit, R., and Erre, R., 1999, Elemental sulfur at the pyrite surfaces: speciation and quantification: Applied Surface Science, v. 143, p. 229–237, doi: 10.1016/S0169-4332(98)00918-0.